



---

**FeS<sub>2</sub> deposited on 3D-printed carbon microlattices as free-standing electrodes for lithium-ion batteries**

Journal:	<i>ChemComm</i>
Manuscript ID	CC-COM-03-2024-001202.R1
Article Type:	Communication

SCHOLARONE™  
Manuscripts

## FeS<sub>2</sub> deposited on 3D-printed carbon microlattices as free-standing electrodes for lithium-ion batteries

Received 00th January 20xx,  
Accepted 00th January 20xx

DOI: 10.1039/x0xx00000x

Cameron Romero,<sup>a</sup> Zhi Liu,<sup>a</sup> Kenneth Gordon,<sup>a</sup> Xiaobo Lei,<sup>b</sup> Karius Joseph,<sup>a</sup> Emily Broussard,<sup>a</sup> Daniel Gang,<sup>b</sup> Zhen Wei,<sup>a</sup> and Ling Fei<sup>a\*</sup>

**We introduce free-standing FeS<sub>2</sub>/carbon microlattice composites as electrodes for lithium-ion batteries through 3D printing. The computer-aided design allows for any shape. The microlattice features aligned microchannels, promoting ion transfer, while carbon skeleton facilitates electron transfer. Overall, this study shows 3D printing is highly promising in advancing sustainable energy applications.**

Advancements in technology in conjunction with rising concerns about global warming have led researchers to search for sustainable and environmentally friendly energy sources.<sup>1-3</sup> Wind and solar are promising alternatives; however, storage of these renewable energies poses a significant threat to their viability.<sup>4-7</sup> Batteries serve as ideal candidates for mitigating their intermittent nature, functioning as an excellent storage medium to receive energy during periods of low energy demand and release it during high-demand times.<sup>8-10</sup> In order to meet energy demands, batteries must exhibit high capacity, power, and safety at an affordable cost, leading researchers in pursuit of more advanced solutions in materials and technologies (e.g., silicon, solid-state electrolytes, etc.).<sup>11-14</sup> Nevertheless, the goal of achieving a high-performance, low-cost battery remains.

Traditional electrodes in batteries are made by slurry coating process.<sup>15-18</sup> This method is known for being time-consuming and tedious since there is a need for mixing, coating, drying, cutting, etc. Furthermore, it faces significant challenges in creating thicker electrodes, such as binder migration to the surface and limited ion diffusion.<sup>19, 20</sup> In contrast, free-standing electrodes present a more efficient and rapid alternative, bypassing the need for solvents and binders, as well as eliminating steps such as drying and coating.<sup>21</sup> This approach

not only streamlines production, but also enables the creation of electrodes with advantageous architecture, greatly boosting battery performance through enhanced mass and charge transfer.<sup>22</sup>

Stereolithography (SLA) 3D printing has recently garnered a lot of attention in academic research since it's relatively affordable ( $\approx$ 450 USD) and has a high pixel resolution ( $>10\ \mu\text{m}$ ).<sup>12</sup> Thanks to this resolution, intricate and precise morphologies can be achieved, in contrast to the slurry method, which only yields a coating film without control over the film's structures. During the printing process, ultraviolet (UV) light solidifies a photocurable resin consisting of photoinitiators, liquid monomers, and oligomers in a pre-programmed shape. This process is repeated layer-by-layer until the build is complete.<sup>23</sup> These printed builds can be carbonized by pyrolysis under an inert atmosphere at a high temperature without destroying the morphology. As such, 3D-printed carbon microlattices with submillimeter unit cells have been reported.<sup>24</sup> Katsuyama et al. created free-standing carbon lattices for sodium-ion batteries and achieved high specific capacity, demonstrating its great potential for metal-ion batteries.<sup>12</sup> Be that as it may, the reported carbon lattices alone do not possess enough capacity for practical applications; however, materials of higher capacity, could address these concerns and render the composite material feasible.

In light of these concerns, the investigation of high-capacity materials for composite integration with the carbon lattice emerges as a pivotal avenue for enhancing energy storage performance. Iron disulfide (FeS<sub>2</sub>) is an attractive solution due to its high theoretical capacity (890 mAh g<sup>-1</sup>), low environmental impact, and affordable cost.<sup>25-27</sup> For example, Zhang et al. developed a carbon-coated FeS<sub>2</sub> composite that served as anode material and reached 495 mAh g<sup>-1</sup> after 50 cycles at 44.5

<sup>a</sup> Department of Chemical Engineering, University of Louisiana at Lafayette, LA 70504, USA.

<sup>b</sup> Department of Civil Engineering, University of Louisiana at Lafayette, LA 70504, USA.

† Footnotes relating to the title and/or authors should appear here.

Electronic Supplementary Information (ESI) available: [details of any supplementary information available should be included here]. See DOI: 10.1039/x0xx00000x

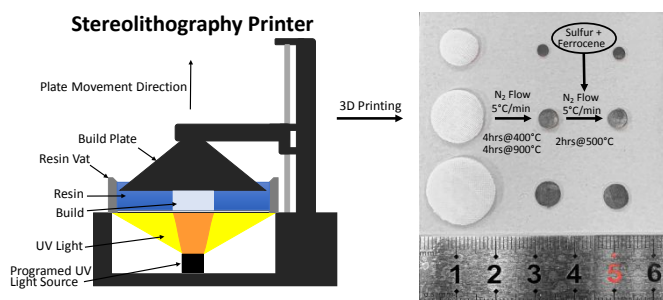


**Figure 1** Schematic illustration of the FeS<sub>2</sub>@Carbon synthetic procedure.

mA g<sup>-1</sup>.<sup>25</sup> Encouragingly, Du et al. used reduced graphene oxide-wrapped FeS<sub>2</sub>, which exhibited a capacity of 1720 mAh g<sup>-1</sup> at a current density of 0.2 A g<sup>-1</sup> after 700 cycles.<sup>26</sup> However, past reports either have documented unsatisfactory cycling stability or rely on slurry coating for electrode preparation. To date, there have been no reports of FeS<sub>2</sub> combined with 3D-printed free-standing electrodes.

Herein, we use SLA 3D printing to create architected carbon microlattices, which act as templates for depositing FeS<sub>2</sub>, thereby creating free-standing composite electrodes for lithium-ion batteries. This method provides several key benefits: (i) computer-aided design flexibility allows for any shape or geometry; (ii) the structure exhibits a high level of repeatability with very little standard deviation due to the exceptional resolution of the 3D printer; (iii) the aligned microchannels along the thickness direction facilitates ion transfer while carbon skeleton aids with electron transfer throughout the entire electrode; (iv) the active material, FeS<sub>2</sub>, exhibits a high theoretical capacity. Profiting from the aforementioned benefits, the engineered electrodes demonstrated impressive cycling performance and rate capability. Specifically, the FeS<sub>2</sub>@Carbon maintained 548 mAh g<sup>-1</sup> after 200 charge/discharge cycles with a current density of 500 mA g<sup>-1</sup>, and a high-rate capability of 743 mAh g<sup>-1</sup> at a current density of 1000 mA g<sup>-1</sup> after the 40<sup>th</sup> cycle. This simple yet effective approach offers valuable insight into the future of novel electrode design for lithium-ion batteries.

The synthetic procedure of FeS<sub>2</sub>@Carbon material is briefly summarized in Figure 1. The models were created in SolidWorks, spliced, and printed using an SLA 3D printer. The as-printed lattices then underwent a two-step carbonization process, followed by the deposition of FeS<sub>2</sub> through annealing at 500°C, all taking place in an N<sub>2</sub> atmosphere, resulting in the final FeS<sub>2</sub>@Carbon samples. The sulfur/ferrocene mixture was in excess in an attempt to completely coat the surface.

During annealing, the ferrocene, a sandwich compound with a central Fe atom bounded to two cyclopentadienyl rings, and sulfur react with each other to form FeS<sub>2</sub> spheres. Meanwhile, cyclopentadienyl rings transform into a carbon layer that envelops FeS<sub>2</sub>, resulting in strengthened structural integrity and improved conductivity. It is important to note that since ferrocene and sulfur turn into vapor phase at elevated temperatures, they can be easily and uniformly deposited on the surface of the 3D printed carbon template.<sup>27</sup>

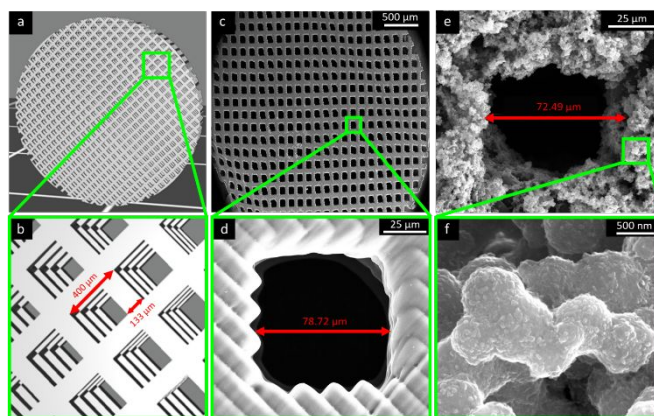


**Figure 2** (a) 3D model of the microlattice disk and (b) its unit structure; (c) SEM image of the carbon microlattice disk and (d) its individual void size; (e) SEM image of FeS<sub>2</sub>@Carbon void size and (f) the individual carbon layer coated FeS<sub>2</sub>.

To understand the crystallinity and phase structures of the obtained samples, XRD (Figure S1a) first confirmed the synthesis of FeS<sub>2</sub>. Raman spectroscopy (Figure S1b) further identified the formation of FeS<sub>2</sub> and provided information on the properties of the carbon material. XPS (Figure S1c-f) was also conducted to illustrate the surface compositions and the corresponding electronic states. Detailed analysis is available in the supporting information.

The digitally designed model with 25 unit cubes in diameter is depicted in Figure 2a. The lattice architecture with channels allows for loading of active material and fast diffusion for the lithium ions in the electrolyte to the electrodes via the channels. The design is disk shaped in order to optimally fit inside of coin cells. Prior to slicing the model, the disk was tilted 90° in the x-axis and 45° in the y-axis to minimize the sections that are orthogonal to the build plate, as these kinds of sections have been shown to produce defects in the final print.<sup>28</sup> The individual dimensions of the unit cubes are displayed in Figure 2b, showing that the distance from one void opening to its adjacent opening is 400 μm and the standard beam thickness is 133 μm. The selection of these dimensions was based on previous findings, which states that the rate performance tends to improve when the feature sizes are reduced. However, limitations exist within printing resolutions that prohibit going any smaller than what was studied.<sup>12</sup>

The morphology of the pyrolyzed microlattice disk was observed with SEM and is depicted in Figure 2c. One important note is that the final shape tends to become oblong. Since the dimensions of the unit cubes were minimized as much as possible, little structural support exists while printing occurs. As the build plate moves up and down to infill more resin, this causes slight vertical compression across the entire build, but negligible compression within individual unit cubes. As can be seen in Figure 2d, the void spaces within the pyrolyzed disks are square, with a void opening of approximately 78.72 μm. This suggests that the overall shape of the disk shrunk by 70–75% after pyrolysis. Figure 2e shows the void space of the annealed FeS<sub>2</sub>@Carbon material. Here, it is important to note that the void opening was reduced to 72.49 μm due to the deposition of

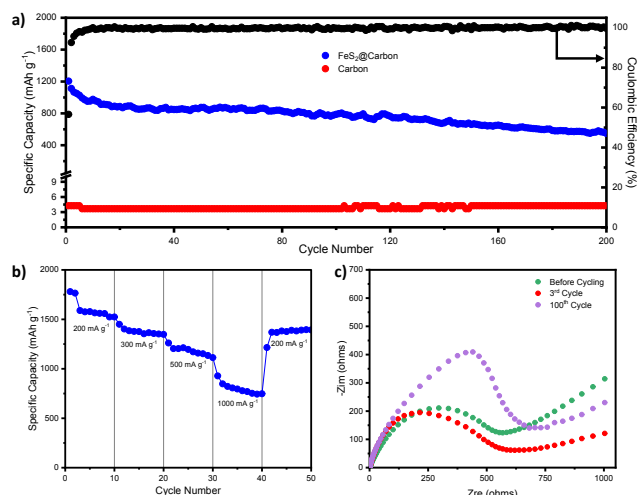


**Figure 3** (a) Cycling stability of carbon and FeS<sub>2</sub>@Carbon with Coulombic efficiency analysis for FeS<sub>2</sub>@Carbon over 200 cycles at 500 mA g<sup>-1</sup>; (b) rate capability of FeS<sub>2</sub>@Carbon; (c) EIS of FeS<sub>2</sub>@Carbon tested at open circuit potential.

the active material. Furthermore, the FeS<sub>2</sub> material appears to be well dispersed and coated on the carbon template surface. The cross-sectional SEM image of the electrode and EDX are shown in Figure S2 and S3. An up-close image of the FeS<sub>2</sub> can be seen in Figure 2f, showing connected spheres of various sizes. The larger spheres have a diameter of ~828 nm while the smaller spheres have a diameter of ~457 nm and are connected together to create a form that mimics a dumbbell shape. Individual FeS<sub>2</sub> can be observed in TEM (Figure S4). The FeS<sub>2</sub>@Carbon has a BET specific surface area of 39.56 m<sup>2</sup>/g, compared to 13.34 m<sup>2</sup>/g for carbon lattice. The disparity in surface area could be attributed to the deposited FeS<sub>2</sub> forming nanostructures on the carbon template, resulting in a highly textured and tortuous surface.

Gravimetric capacity is an important criterion for electrode materials.<sup>29–32</sup> The as-synthesized FeS<sub>2</sub>@Carbon was assessed on its gravimetric specific capacity and long-term cycling stability. As displayed in Figure 3a, the cycling stability of the FeS<sub>2</sub>@Carbon and carbon templates are both steady up to 200 cycles at a current density of 500 mA g<sup>-1</sup>; however, at the 200<sup>th</sup> cycle, the specific capacity of the carbon template is negligible (3.66 mAh g<sup>-1</sup>) compared to the composite material (562.5 mAh g<sup>-1</sup>). The low capacity of carbon microlattice alone could be due to the lack of micro/meso pores, which limits ion transfer into its internal structure. This indicates the critical role of the free-standing carbon lattice as an excellent support as well as the necessity of depositing the active material on its surface to achieve high capacity. Additionally, the FeS<sub>2</sub>@Carbon material maintains a Coulombic Efficiency >99% after ten cycles. The composite's good cycle performance at intermediate current density demonstrates the robust nature of FeS<sub>2</sub> spheres and the integrity of carbon microlattice as support. Exploration on the size-dependent performance of the 3D printed materials was conducted (Figure S5) as well as cycling stability at higher current densities (Figure S6).

Rate capability test was performed to evaluate the electrode's capability of fast Li-ion transfer and storage.<sup>33–35</sup> As displayed in

Figure 3b, the FeS<sub>2</sub>@Carbon material delivers a 10<sup>th</sup> cycle capacity of 1524 mAh g<sup>-1</sup> at 200 mA g<sup>-1</sup>, 1348 mAh g<sup>-1</sup> at 300 mA g<sup>-1</sup>, 1113 mAh g<sup>-1</sup> at 500 mA g<sup>-1</sup>, 748 mAh g<sup>-1</sup> at 1000 mA g<sup>-1</sup>, and 1393 mAh g<sup>-1</sup> at the returning 200 mA g<sup>-1</sup>. When the current density returned to its initial value, the majority of the capacity was recovered (only 131 mAh g<sup>-1</sup> loss over 50 cycles), showing good rate capability. These findings suggest that the material is structurally stable, and because the channels are oriented along the thickness direction, facilitating the rapid penetration of electrolyte and, in turn, providing easy access for lithium ions to reach active material sites. Simultaneously, the interconnected carbon microlattice skeleton supports efficient electron transport across the entire electrode.<sup>36, 37</sup>

To investigate the interfacial properties, especially SEI formation of the materials, electrochemical impedance spectra were recorded for coin cells before and after cycling. As shown in Figure 3c, the Nyquist plots of the FeS<sub>2</sub>@Carbon electrode prior to cycling, after 3 cycles, and after 100 cycles are presented. At all stages of cycling, the material exhibits a single semicircle in the high frequency region, and a slope line in the low frequency region. The semicircle is primarily related to the charge transfer resistance at the electrode-electrolyte interface. The larger the diameter, the greater the charge transfer resistance, indicating slower transfer kinetics at the interface.<sup>38, 39</sup> From the figure, it can be seen that the diameter slightly increases from the 0 cycle to 3 cycle, and increases even further when looking at the 100 cycle sample. This is because of the formation of the SEI on the materials surface; however, the change is minimal. In the low frequency region, the pseudo-linear line corresponds to the mass transport in the electrode. When this line makes a 45° angle with the real axis, it is known as a Warburg element, which indicates semi-infinite linear diffusion at low frequencies. When this angle is <45°, as can be seen in our results, this indicates that there is a limited diffusion layer.<sup>40–42</sup> As the cycles increase, the slope of the line decreases, indicating that the processes is increasingly deviating from the ideal case. Be that as it may, the change in the slope is minimal. These minimal changes can again be reasonably attributed to the designed architecture that the aligned channels along the thickness of the electrode allow for efficient ion transfer and carbon skeletons for fast electron transfer.<sup>43, 44</sup> An equivalent circuit model with fitted values and analysis can be found in Figure S7. To further understand the lithium storage mechanism of the FeS<sub>2</sub>@Carbon electrodes, stepwise cyclic voltammetry (CV) measurements (0.2–1.0 mV s<sup>-1</sup>) were carried out (Figure S8) with detailed analysis available in supporting information. SEM images after 200 cycles of FeS<sub>2</sub>@Carbon (Figure S9) shows the electrode remains intact without visible breakage or cracks.

In summary, we have successfully deposited FeS<sub>2</sub> on the surface of pyrolyzed, 3D printed, carbon microlattice disks to serve as free-standing electrodes in lithium-ion batteries. The composite material shows promising electrochemical cyclability and rate capability. The auspicious performance is achieved by the well-designed microstructure, which is robust, conductive, and composed of aligned channels that facilitate efficient ion and electron diffusion. Currently, FeS<sub>2</sub> is solely applied to the surface of the carbon template. Some particles may become

less stable during charge and discharge cycles. We anticipate that by embedding the FeS<sub>2</sub> precursor in the resin and thus integrating it within the carbon template, the performance of the electrodes could be further enhanced. The proof-of-concept work also suggests that alternative active materials, aside from FeS<sub>2</sub>, could likewise be integrated in similar fashion. Overall, this study shows the promising role that 3D printing can play in creating free-standing composite electrodes for lithium-ion batteries, advocating for sustainable energy from both a research-driven and practical standpoint.

This research is supported by NASA under 80NSSC21M0333 and LEQSF(2020-24)-LaSPACE, PO-0000246463.

### Data Availability

The data supporting this article have been included as part of the Supplementary Information.

### Conflicts of interest

There are no conflicts to declare.

### References

- M. Zhang, H. Du, Z. Wei, X. Zhang and R. Wang, *ACS Applied Energy Materials*, 2021, **5**, 186-195.
- M. Zhang, A. Nautiyal, H. Du, Z. Wei, X. Zhang and R. Wang, *Electrochimica Acta*, 2021, **376**, 138037.
- M. Zhang, H. Du, Z. Wei, X. Zhang and R. Wang, *ACS Applied Energy Materials*, 2021, **4**, 8262-8274.
- Y. Yang, S. Bremner, C. Menictas and M. Kay, *Renewable and Sustainable Energy Reviews*, 2018, **91**, 109-125.
- Y. Liang, Z. Wei, H.-E. Wang, M. Flores, R. Wang and X. Zhang, *Journal of Power Sources*, 2022, **548**, 232071.
- Y. Liang, Z. Wei, R. Wang and X. Zhang, *Coatings*, 2022, **12**, 1060.
- Y. Liang, Z. Wei, H.-E. Wang, R. Wang and X. Zhang, *Science China Materials*, 2023, **66**, 964-973.
- D. S. Mallapragada, N. A. Sepulveda and J. D. Jenkins, *Applied Energy*, 2020, **275**, 115390.
- S. Azam, Z. Wei and R. Wang, *Journal of Colloid and Interface Science*, 2022, **615**, 417-431.
- S. Azam, Z. Wei and R. Wang, *Journal of Colloid and Interface Science*, 2023, **635**, 466-480.
- F. Zou and A. Manthiram, *Advanced Energy Materials*, 2020, **10**, 2002508.
- Y. Katsuyama, A. Kudo, H. Kobayashi, J. Han, M. Chen, I. Honma and R. B. Kaner, *Small*, 2022, **18**, 2202277.
- Z. Barlow, Z. Wei and R. Wang, *Materials Chemistry and Physics*, 2024, **314**, 128830.
- Z. Barlow, Z. Wei and R. Wang, *Materials Chemistry and Physics*, 2023, **309**, 128316.
- J. Li, J. Fleetwood, W. B. Hawley and W. Kays, *Chemical Reviews*, 2021, **122**, 903-956.
- M.-C. Li, Z. Liu, L. Tan, Q.-Y. Zhou, J.-J. Zhang, P.-P. Hou, X.-J. Jin, T.-B. Lv, Z.-Q. Zhao and Z. Zeng, *ACS Sustainable Chemistry & Engineering*, 2022, **10**, 10223-10233.
- Q.-Y. Zhou, L. Tan, T.-B. Lv, M.-C. Li, J.-J. Zhang, Z.-Q. Zhao, X.-J. Jin, Z. Liu, P.-P. Hou and Z. Zeng, *ACS Applied Materials & Interfaces*, 2023, **15**, 3037-3046.
- P. Wu, L. Tan, X.-D. Wang, P. Liao, Z. Liu, P.-P. Hou, Q.-Y. Zhou, X.-J. Jin, M.-C. Li and X.-R. Shao, *Materials Research Bulletin*, 2022, **145**, 111550.
- L. Zolin, M. Chandesris, W. Porcher and B. Lestriez, *Energy Technology*, 2019, **7**, 1900025.
- Z. Zhao, M. Sun, W. Chen, Y. Liu, L. Zhang, N. Dongfang, Y. Ruan, J. Zhang, P. Wang and L. Dong, *Advanced Functional Materials*, 2019, **29**, 1809196.
- L. Zeng, P. Li, Y. Yao, B. Niu, S. Niu and B. Xu, *Materials Today Nano*, 2020, **12**, 100094.
- S.-j. He, K.-q. Zhang, Y.-j. Zou and Z.-h. Tian, *New Carbon Materials*, 2022, **37**, 898-917.
- T. D. Ngo, A. Kashani, G. Imbalzano, K. T. Nguyen and D. Hui, *Composites Part B: Engineering*, 2018, **143**, 172-196.
- A. J. Jacobsen, S. Mahoney, W. B. Carter and S. Nutt, *Carbon*, 2011, **49**, 1025-1032.
- D. Zhang, Y. Mai, J. Xiang, X. Xia, Y. Qiao and J. Tu, *Journal of Power Sources*, 2012, **217**, 229-235.
- Y. Du, S. Wu, M. Huang and X. Tian, *Chemical Engineering Journal*, 2017, **326**, 257-264.
- L. Fei, Y. Jiang, Y. Xu, G. Chen, Y. Li, X. Xu, S. Deng and H. Luo, *Journal of Power Sources*, 2014, **265**, 1-5.
- H. Quan, T. Zhang, H. Xu, S. Luo, J. Nie and X. Zhu, *Bioactive materials*, 2020, **5**, 110-115.
- Y. Huang, Y. Fang, X. F. Lu, D. Luan and X. W. Lou, *Angewandte Chemie*, 2020, **132**, 20086-20090.
- L. L. Lu, Y. Y. Lu, Z. X. Zhu, J. X. Shao, H. B. Yao, S. Wang, T. W. Zhang, Y. Ni, X. X. Wang and S. H. Yu, *Science Advances*, 2022, **8**, eabm6624.
- Y. An, Y. Tian, C. Liu, S. Xiong, J. Feng and Y. Qian, *ACS Nano*, 2022, **16**, 4560-4577.
- S. Wang, B. Y. Guan, L. Yu and X. W. Lou, *Advanced Materials*, 2017, **29**, 1702724.
- Z. Wei, J. Li, Y. Wang and R. Wang, *Electrochimica Acta*, 2021, **388**, 138645.
- Z. Wei, J. Li and R. Wang, *Applied Surface Science*, 2022, **580**, 152237.
- Z. Wei and R. Wang, *Journal of Colloid and Interface Science*, 2022, **615**, 527-542.
- S. Hwang, D. Lee, Y. Rho, K. S. Yoon, D. M. Yu, S. J. Yoon, S. Kim, Y. T. Hong and S. So, *Journal of Power Sources*, 2021, **489**, 229497.
- H. Cheng, R. Xiao, H. Bian, Z. Li, Y. Zhan, C. K. Tsang, C. Chung, Z. Lu and Y. Y. Li, *Materials Chemistry and Physics*, 2014, **144**, 25-30.
- N. E. Tolouei, S. Ghamari and M. Shavezipur, *Journal of Electroanalytical Chemistry*, 2020, **878**, 114598.
- A. Ali, S. Sarwar, D. R. Pollard, Z. Wei, R. Wang, X. Zhang and A. J. Adamczyk, *The Journal of Physical Chemistry C*, 2022, **126**, 17011-17024.
- B. Yin, X. Cao, A. Pan, Z. Luo, S. Dinesh, J. Lin, Y. Tang, S. Liang and G. Cao, *Advanced Science*, 2018, **5**, 1800829.
- H. S. Magar, R. Y. Hassan and A. Mulchandani, *Sensors*, 2021, **21**, 6578.
- P. Córdoba-Torres, T. J. Mesquita and R. P. Nogueira, *The Journal of Physical Chemistry C*, 2015, **119**, 4136-4147.
- S. Fahad, Z. Wei and A. Kushima, *Journal of Power Sources*, 2021, **506**, 230175.
- Z. Wei, S. Sarwar, S. Azam, M. R. Ahasan, M. Voyda, X. Zhang and R. Wang, *Journal of Colloid and Interface Science*, 2023, **635**, 391-405.

### **Data Availability Statement**

All the important data has been presented in the main manuscript. The experimental data supporting this article have been included as part of the Supplementary Information.